Supplementary information

Magneto-structural properties of rhombohedral Ni and Ni-B nanotubes deposited by electroless-plating in track-etched mica templates

Falk Muench,[a†], Sandra Schaefer[a], Miguel Méndez[b], Jose Angel Fernández-Roldán[b], A. Silvia González-García[b], Víctor Vega[c†], Ulrike Kunz[a], Wolfgang Ensinger[a], Javier García[b], Víctor M. Prida[b]

[a.] *Technical University of Darmstadt, Department of Materials and Earth Sciences, Alarich-Weiss-Straße 2, 64287 Darmstadt, Germany.*
[b.] *Physics Department, University of Oviedo. C/ Federico García Lorca nº 18, 33007-Oviedo, Spain.*
[c.] *Laboratory of Nanoporous Membranes, Scientific-Technical Services of the University of Oviedo. Campus El Cristo s/n, 33006- Oviedo, Spain.*
† Corresponding authors, e-mail address: F.M.: muench@magnotherm.com; V.V.: vegavictor@uniovi.es.

Micromagnetic modelling of Ni and Ni-B nanotubes.

The magnetic hysteresis loops of amorphous Ni-B rhombic nanotubes were evaluated with lengths of 1 and 5 micron assuming the material as a mixture of a non-magnetic and magnetic (granular) phase. We observed an isotropic response irrespective of the applied field direction and a quasi-superparamagnetic behaviour of the magnetic phase.

1. Model of Ni-B and Ni

Previous studies of electrodeposited amorphous Ni-B on Si substrates performed with Inductively Coupled Plasma-Mass-Spectrometry (ICPMS) technique confirm a 25-26% B content for which this alloy consists of a matrix of most non-magnetic atoms [1]. Several characterization studies [1,2] of bulk amorphous and liquid Ni-B alloys suggest that this specific composition is formed by a segregation of a predominant non-magnetic Ni_2B phase and a diluted Ni phase although there is not confirmation in individual electroless-deposited nanotubes of Ni-B with similar geometries and dimensions to our knowledge.

To enlighten (1) the material nanostructure of Ni-B rhombic nanotubes, (2) its magnetic response and (3) to deepen the magnetic structure behind the remagnetization process, we have performed a micromagnetic modelling of individual nanotubes. Importantly, the large distance between closest nanotubes and the low saturation magnetization reported in VSM measurements allow the restriction of the modelling to individual nanotubes in terms of magnetostatic interaction without loss of generality. Our micromagnetic model of Ni and Ni-B nanotubes with mumax3 [3-5], assumes a 3D Voronoi granular distribution of the nanotube volume with grain mean size of 10 nm, where 1.3% of the grains are considered of Ni. This ratio is selected due to low signal of Ni-B compared to Ni in magnetometry measurements. We have used standard material parameters of Ni such as a spontaneous magnetization value of 2.45×10^5 A/m and an exchange stiffness of 1.9×10^{-12} J/m. We have considered a maximum nanotube length of 5 μm. The major and minor diagonals of the rhombic base of nanotube are 590 and

360 nm long respectively, and a wall thickness of 44 nm close to the dimensions obtained from Scanning Electron Microscopy.

The rhombic nanotube volume considered for the micromagnetic model shown in Figure S1 has been discretized in 255 regions with mean size of 10 nm and standard deviation 10 nm to model the magnetic/ non-magnetic matrix. 1.3% of these grains are considered Ni with the experimental properties described in the main text in agreement with the low magnetic signal obtained from VSM measurements. The maximum discretization size was between 2 and 5 nm for Ni-B, and between 5 and 7 nm for the Ni nanotube.

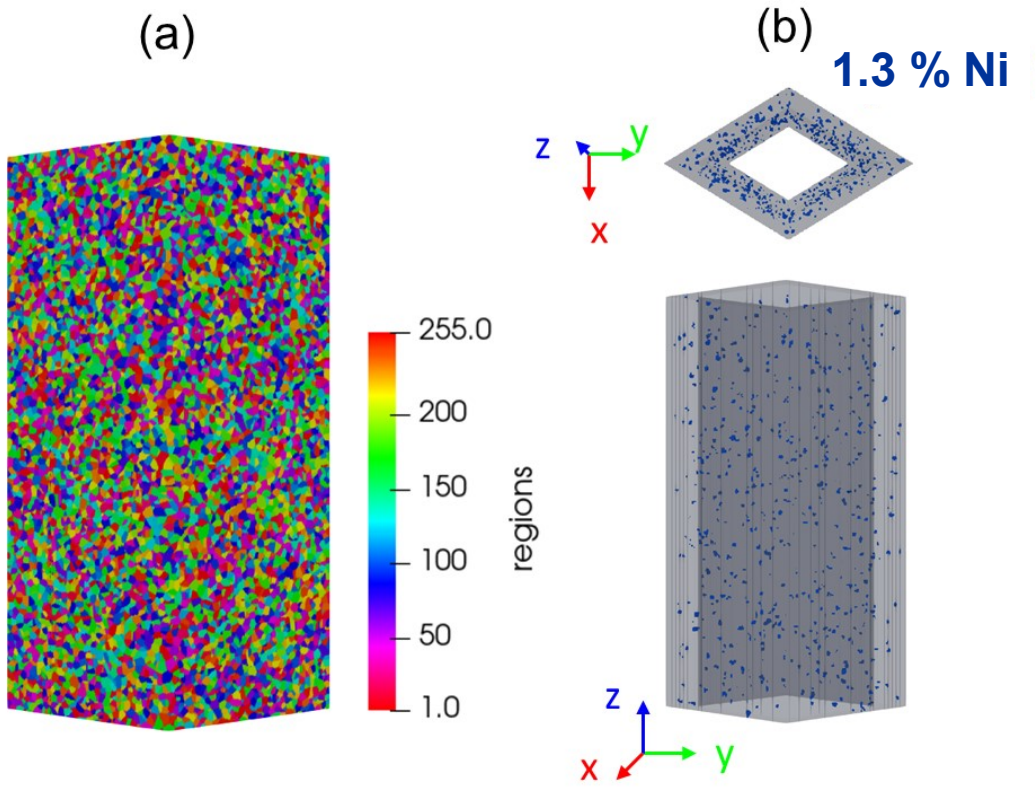

Figure S1. (a) Geometry and volume of a hollow rhombic prism discretized in 255 sets of grains by a Voronoi algorithm. (b) The matrix of the non-magnetic phase is displayed in grey color having 1.3 % of the total volume filled with Ni grains.

2. Ni-B nanotube

2.1. Coherent rotation of superparamagnetic domains in grains

The energy interplay between exchange and demagnetization during the remagnetization process displayed in the hysteresis loops of Figure S2(a) confirm a quasi-superparamagnetic behaviour of the Ni-B, where each grain adopts a single domain state as evinced by the null exchange energy. The different maximum values of the demagnetizing energy obtained in Figure 2(a-c) evinces a shape anisotropy emerging from the overall granular structure despite the dilution of the magnetic phase in the nanotube. While the specific orientation of the single domains at remanence depends on the geometry of each grain, the total demagnetizing energy

in Ni-B nanotubes indicates a favourable orientation in the inverse order, i.e. (1st) along the direction of the larger direction of the diagonal and (2nd) along the axis of the nanotube. In both nanotubes the direction of the shorter diagonal is a 'hard magnetic axis'. This effect is not so evident in shorter Ni-B nanowires, and it remains as an open question if tailoring the Ni-B with a specific granular texture could induced a designed orientation of the easy magnetization axis along any other direction.

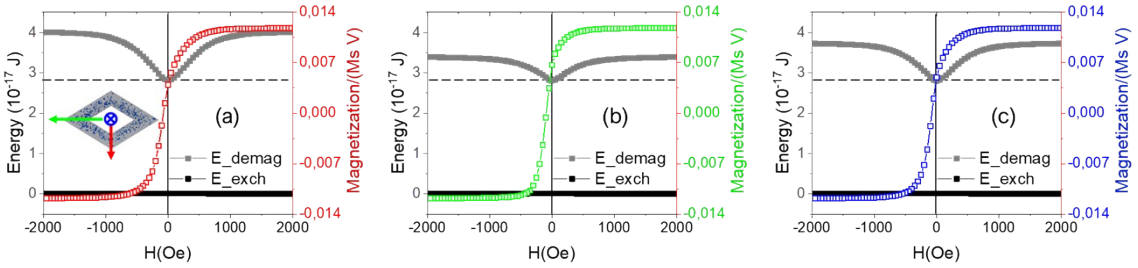

Figure S2. Demagnetizing and exchange anisotropy energies in the hysteresis loops as function of the magnetic field applied parallel to the axis of the 5 µm long NiB nanotube (a) and parallel to the long (b) and short (c) diagonals of the rhombic base. In red, green and blue one branch of the hysteresis loop with field applied along the axis directions.

Overall, (1) the isotropic magnetic response of the rhombic matrix provides important implications and appealing properties for applications which require a low net magnetic moment, low (and directional) stray fields and anhysteretic response such as encapsulation of nanoparticles for drug delivery, arrays of non-interacting nanotubes with low magnetic moments and stray fields, or magnetic nanocarriers directionally oriented under applied magnetic fields with low amplitude values.

It is generally assumed that low and vanishing magnetostatic dipolar interactions, and long-range exchange magnetic interactions are assumed to play an insignificant role in the magnetic response of magnetic systems at the nanoscale. Here we provide a geometry where the dilution of a magnetic phase induces (1) a quasi-superparamagnetic response and (2) the exchange of the orientations of the easy axis of magnetization despite a vanishing dipolar coupling. This example highlights the importance of considering long range dipolar interactions in applications based on magnetic nanostructured systems and 3D nanoarchitectures which are sensitive to low stray fields.

2.1. Intergrain exchange coupling in Ni-B nanotubes

Importantly, we have observed a global isotropic magnetic behaviour irrespective of the direction of the applied field and length independent over 1 µm in the reversal process. With this shift in focus, we have restricted the following studies to a length of 1 µm for fundamental studies.

The insignificant role of the intergrain exchange coupling among neighbouring grains is confirmed by the overlapping hysteresis loops where reductions up to 80% of exchange coupling have been considered, irrespectively of the applied field direction. The low intergrain exchange coupling is additionally promoted by the low density of Ni grains (See Figure S3(a-d)).

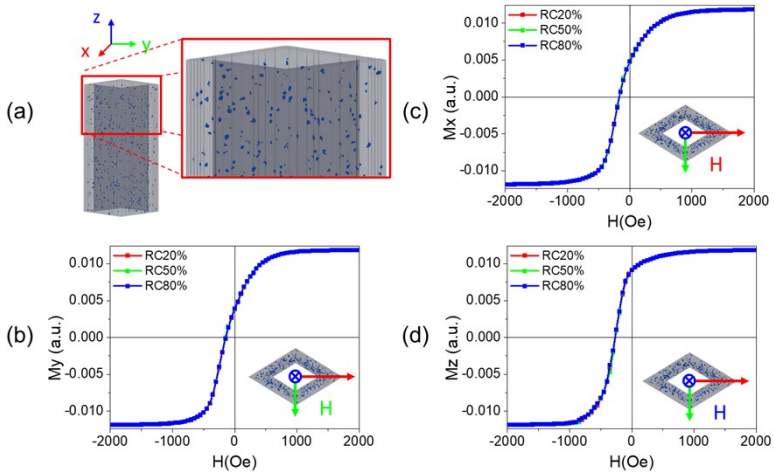

Figure S3. (a) Zoom view of the granular structure in the 1 µm long Ni-B nanotube. Grains are coloured by dark blue. (c-d) Hysteresis loops of the Ni-B nanotube with field applied along the x, y and z directions as a function of the intergrain exchange coupling. These loops include a cubic magnetocrystalline anisotropy $K_{c1}=10^4$ Jm^{-3} with [111] direction parallel to the nanotube axis.

3. Magnetic states in the Ni nanotube

3.1 Field applied along the Z-axis (nanotube axis)

The hysteresis loop is evaluated with the magnetic field applied in the direction of the longitudinal axis resulting in a total orientation of the magnetic domains along the Z-axis (Fig S4a). When the field strength is decreased, the reversal in the nanotube occurs through the nucleation of vortex states at both ends of the nanotube (Fig. S4b). The magnetization switching process takes place through the depinning and propagation of both domain wall vortices starting from the ends of the nanotube towards its centre (Fig. S4c). A single Barkhausen jump is thus observed in the hysteresis loop with high remanence value.

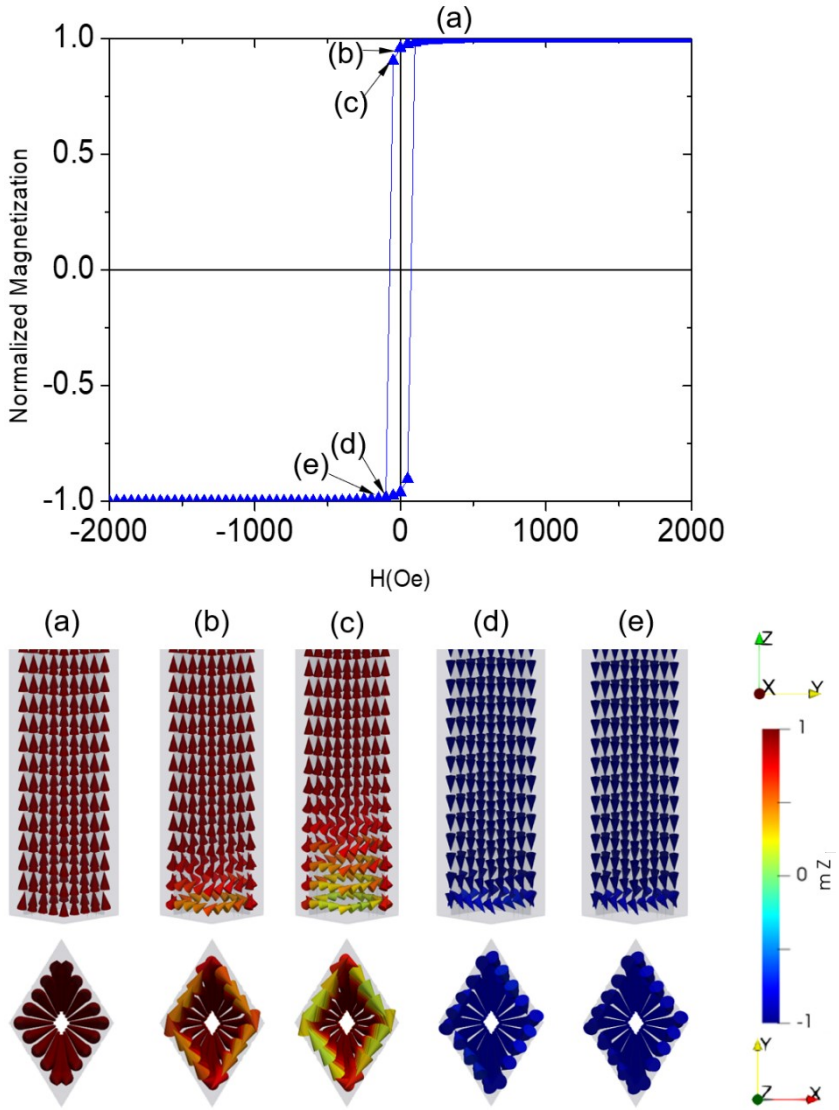

Figure S4 Hysteresis loop for the applied magnetic field along the Z axis (axial direction of the rhombic nanotube), representing the reversal magnetization process along the longitudinal axis. (a) Partial nanotube with total saturation. (b) Vortex appearing on edges of the nanotube. (c) Remanence, vortex propagating into the nanotube. (d) First step of the inversion of magnetization. (e) Nanotube nearly in saturation.

3.2 Field applied along the X-axis (minor diagonal of the rhombic basis)

When the magnetic field is applied in the direction of the minor diagonal of the basis, the hysteresis loop exhibits a lower slope, with much lower remanence and coercive field values than when the field was applied along the longitudinal axis.

As the field decreases, magnetization rotation processes are small and exert no appreciable effect until you reach the state of figure S5(a), where a 'onion-like' magnetic configuration is formed at the ends of the tube. As the field decreases further, an antivortex state appears on the nanotube surface (Fig S5b). Importantly, there is a field value where the magnetization pointing outwards from the nanotube propagates along the edge to close the field lines (Fig S5c). At the opposite end there is also an "inwards" point of the magnetization into the nanotube. After this event, it can be seen how a very small Barkhaussen jump appears in the hysteresis

loop. This magnetization jump is evidence of an energetic change in the arrangement of the magnetic domains that are reoriented (front figures S5c to S5d), which is the precursor to the formation of two vortices at the ends of the nanotube (Fig S5f) that propagate along the nanotube to give rise to Fig S5g. At higher fields, the reversal process completes through the rotation of magnetic moments (fig S5h).

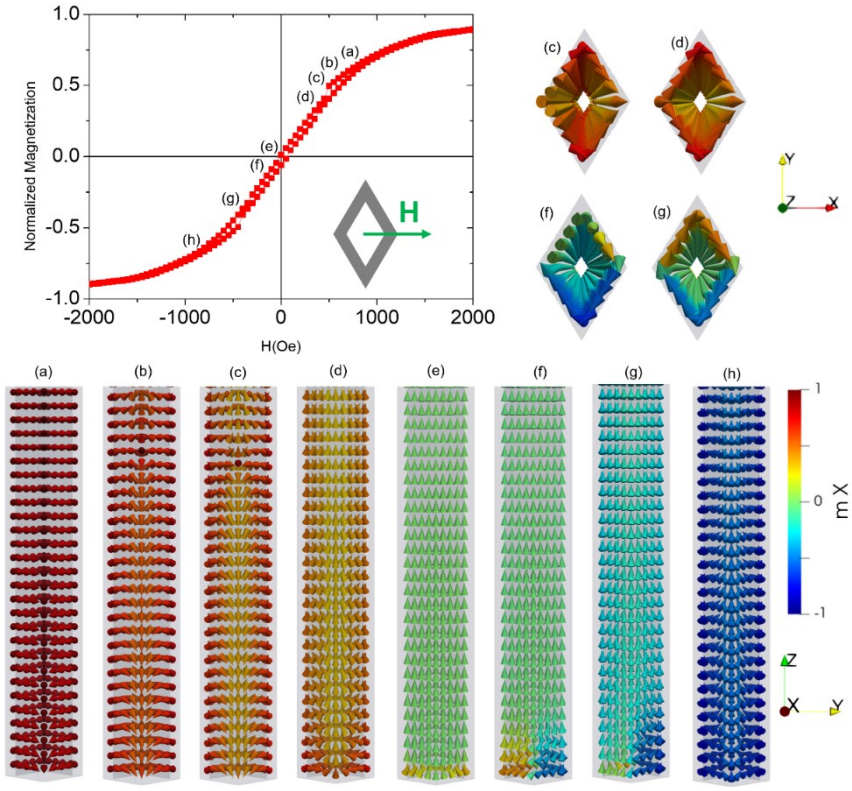

Figure S5. Hysteresis loop with the applied magnetic field along the X direction (shorter diagonal of Ni nanotube). (a-h) Evolution of nanotube magnetization during the reversal process. (c,d,f,g – up) Frontal view of nanotube edge.

3.3 Field applied along the Y-axis (major diagonal of the rhombic basis)

With magnetic field applied in the direction of the rhombic nanotube's major diagonal axis, full saturation is reached with lower field values than for the case of the field applied along the minor diagonal, evincing a lower configurational anisotropy induced by the irregular basis.

Figure S6a shows the nanotube with the magnetic domains completely oriented in the Y-axis direction. The transition from (a) to (b) takes place more quickly and the formation of a transverse domain wall can be observed (Fig S6b). Although it has not been observed, the formation of an antivortex state as in the previous case cannot be discarded for other directions of the applied field. Here the reversal process does not result in the formation of two vortices at the ends of the tube. In the same figure (Fig S6d) it can be seen how almost the entire magnetization of the nanotube is oriented in the Z direction except for the ends, which give rise, on this occasion, to an "S-state" at point (d), in the remanence. Further decreasing the field causes the reversal of the magnetization at the nanotube ends, producing a rotation through the walls of the remaining moments (which until now were pointing in the Z-axis, in Fig S6e). At

the points (f, g and h) of Figure S6, the field continues decreasing until the magnetization of the Ni nanotube is completely reversed.

An important remark is that between steps (c) and (d), the inversion of a single edge of the rhombic Ni nanotube occurs.

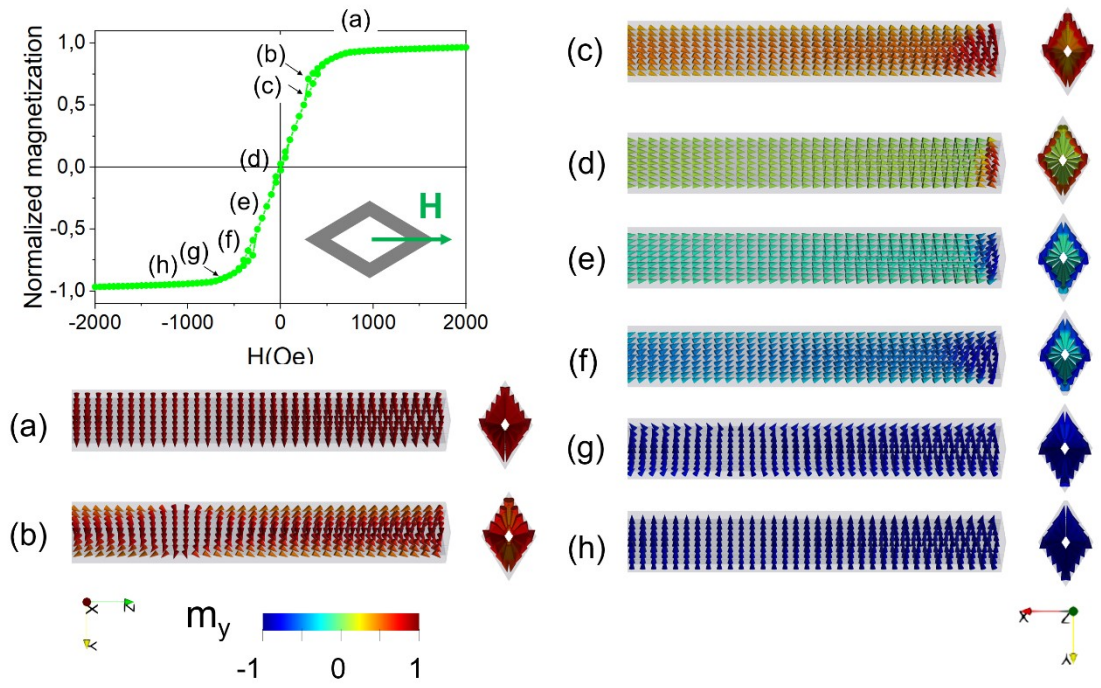

Figure S6. Hysteresis loop with the applied magnetic field along the Y direction (larger diagonal of Ni nanotube). (a-h) Evolution of the nanotube magnetization during the reversal process.

References for SI:

[1] K.I. Portnoi, V.M. Romashov, V.M. Chubarov, M.K. Levinskaya, and S.E. Salibekov, Sov. Powder Metall. Met. Ceram. 6, 99 (1967). DOI: https://doi.org/10.1007/BF00775639

[2] I. Bakonyi, E. Babić, M. Miljak, R. Lück, J. Bahle, R. Hasegawa, and J. Kollár, Phys. Rev. B 65, 104423 (2002). https://doi.org/10.1103/PhysRevB.65.104423

[3] A. Vansteenkiste, J. Leliaert, M. Dvornik, M. Helsen, F. Garcia-Sanchez and B.V. Waeyenberge, AIP Adv., 2014, 4, 107133. DOI: https://doi.org/10.1063/1.4899186

[4] L. Exl, S. Bance, F. Reichel, T. Schrefl, H.P. Stimming and N.J. Mauser, J. Appl. Phys., 2014, 115, 17D118. DOI: https://doi.org/10.1063/1.4862839

[5] J. Leliaert, B. Van de Wiele, A. Vansteenkiste, L. Laurson, G. Durin, L. Dupré, and B. Van Waeyenberge, J. Appl. Phys., 2014, 115, 233903. DOI: https://doi.org/10.1063/1.4883297